Origin of Differing Reactivities of Aliphatic Chains on H−Si(111) and Oxide Surfaces with Metal

Christina A. Hacker,*,† Curt A. Richter,† Nadine Gergel-Hackett,† and Lee J. Richter‡

Semiconductor Electronics Division and Surface and Microanalysis Science Division, National Institute of Standards and Technology, 100 Bureau Drive, Gaithersburg, Maryland 20899

Received: March 20, 2007; In Final Form: April 24, 2007

The interaction of deposited metals with monolayer films is critical to the understanding of, and ultimate utility of, the emerging arena of molecular electronics. We present the results of a thorough study of the interaction of vapor-deposited Au and Ag on alkane films attached to Si substrates. Two distinct categories of films are studied: C18 films formed from the hydrosilation reaction of octadecyl trichlorosilane with thin SiO_2 layers and C18 films formed from the direct attachment of functionalized alkanes with hydrogen-terminated Si. Two direct attachment chemistries were studied: $(Si)_3$−Si−O−C linkages of 1-octadecanol and octadecanal on H-terminated Si(111) and $(Si)_3$−Si−C linkages of 1-octadecene on H-terminated Si(111). The reactivity of the films was studied with p-polarized backside reflection absorption spectroscopy (pb-RAIRS), sputter depth profiling X-ray photoelectron spectroscopy (XPS), spectroscopic ellipsometry (SE), atomic force microscopy (AFM), and device electrical tests. Independent of direct attachment chemistry, we report the remarkable observation that deposition of Au results in the displacement of the molecular film from the Si interface. In contrast, the directly attached molecular films are robust toward the deposition of Ag. For both metals, the C18 films formed by hydrosilation reactions on SiO_2 remain at the interface. The results of monolayer stability with metal are linked to reactions between the metal and substrate. The displacement of the films by Au is attributed to Au insertion in the Si backbonds, in a reaction analogous to silicide formation. The results demonstrate that one must fully take into account the reactivity of the entire system, including substrates, molecular functional groups, and metal electrodes, when considering the robustness of molecules in metal junctions.

Introduction

The formation of the top metal electrode for molecular electronics is a challenging step in making electrical test structures on the basis of organic monolayers. Often, instead of the idealized metal/organic−monolayer/substrate system, the actual structure consists of multiple metal filaments that penetrate through the organic monolayer and dominate the electrical response.[1−5] To reduce the amount of metal penetration, researchers have examined the use of a thin reactive metal, such as Ti, Cr, or Ni, to form a diffusion barrier.[6−10] The Ti reacts with the organic monolayer to form either Ti−O or Ti−C at the metal−organic interface and thus prevents the diffusion of Au, Al, or other metals into the organic monolayer at the expense of the integrity of the monolayer. Much work in recent years has been aimed at understanding the best way to form the top metal electrode. Approaches include special metal deposition conditions,[11−14] selective use of the top functional groups,[15−18] and the use of thin reactive metal layers.[6−8,19,20]

After formation of electrical structures, however, it is very difficult to characterize the chemical and physical structure of the device. Metal thicknesses of more than 5−10 nm render the underlying organic monolayer invisible to optical and charge particle techniques. Typically, the properties of the actual test structure are extrapolated from studies made by using metal thin enough to be transparent to these techniques. We have recently described the use of p-polarized backside reflection absorption infrared spectroscopy, pb-RAIRS, which enables characterization of the organic film under thick metal electrodes.[21] This technique relies on the infrared-transparent nature of the silicon substrate with tethered organic monolayers and an infrared reflective metal electrode on top. Using pb-RAIRS, the surprising result was found that alkoxy monolayers covalently bonded to the Si−H surface are displaced from the interface by Al, Au, and Ti, in contrast to comparable monolayers formed on silicon oxide substrates.[21]

In this paper, we expand the study of the displacement reaction to include both alkoxy (C−O−Si−) and alkane (C−Si−) monolayers and focus on the reactivity of the noble metals Au and Ag. In addition to pb-RAIRS studies of thick (≈100 nm) metal deposits, we employ sputter depth profiling X-ray phototelectron spectroscopy (XPS) (with ≈20 nm metal films) and atomic force microscopy (AFM) and spectroscopic ellipsometry (SE) (with ≈5 nm metal films). We find that the interaction of the metal with the underlying substrate is critical in determining the fate of the directly attached monolayers, independent of attachment chemistry.

Experimental Section

Alkane monolayers from the reaction of octadecyltrichlorosilane (OTS) were formed on double-side polished Si(111) wafers (n-type, P-doped, 8−12 Ω·cm). The wafers were first RCA cleaned followed by a 30 min treatment in a commercial

* To whom correspondence should be addressed. E-mail: christina.hacker@nist.gov.
† Semiconductor Electronics Division.
‡ Surface and Microanalysis Science Division.

10.1021/jp072216u CCC: $37.00 © 2007 American Chemical Society
Published on Web 06/05/2007

UV−ozone cleaner (UVO) to produce ≈1.7 nm thick oxides. OTS monolayers were formed by immersion of the substrates in a 2 mmol/L solution in hexadecane for 18 h. Immediately prior to immersion, the UV−oxide substrates were cleaned by using a 5 min UVO treatment on each side. Upon removal from solution, the samples were cleaned by ultrasonic treatment in chloroform, isopropyl alcohol, and 18 MΩ·cm (DI) water and then were annealed at 150 °C for 10 min. Alkoxy monolayers directly attached to Si were formed by the UV promotion of the reaction of dilute solutions of 1-octadecanol, hereafter referred to as alcohol, in CH_2Cl_2 with the H-terminated Si(111) surface (H−Si) as described previously.[22,23] 1-Octadecene (referred to as alkene) and octadecanal (referred to as aldehyde) functionalized surfaces were prepared by immersing the H−Si(111) substrate in a 1:1 dichloromethane:isooctane-(2,2,4-trimethylpentane) (v:v) solution containing ≈10 mmol/L of the C18 molecule and were maintained at 100 °C for 4 h in a nitrogen glovebox. The resultant films are dense and covalently bonded to the Si(111) substrate. Direct attachment was indicated by the elimination of the Si−H vibrational features. The films were moderately robust to oxidative attack, as no Si−O−Si vibrational features were observed by transmission IR during brief (24 h) exposure to air.

Top metal layers were deposited from physical evaporation sources. The deposition rate was nominally 0.05−0.1 nm/s for the first ≈10 nm and then ≈0.5 nm/s for the remaining deposition. All quoted thicknesses are nominal on the basis of an adjacent quartz-crystal monitor. The evaporator base pressure prior to deposition was 1.3×10^{-4} Pa (10^{-6} Torr) and did not exceed 1.3×10^{-3} Pa (10^{-5} Torr) during evaporation. The sources were ≈60 cm from the target. Blanket metal films were deposited on ≈(15 mm × 15 mm) samples for pb-RAIRS, AFM, and XPS characterization. For the pb-RAIRS measurements with Ag films, only 20 nm of Ag was deposited, followed by a 100 nm Au capping layer to avoid degradation of the Ag film during subsequent processing.

Reference samples were created by deposition of the metals directly on native oxide and on H-terminated Si(111) substrates. The alkane films and metal depositions were performed via batch processing providing a high degree of reproducibility. All infrared spectra were recorded with a commercial Fourier transform (FT) instrument with a HgCdTe (MCT) detector at 8 cm^{-1} resolution collecting 512 coadded scans. P-polarized Brewster angle (≈73.7°) transmission spectra were acquired with a custom-built sample holder. P-polarized, near-Brewster angle, backside reflection spectra were acquired with a commercial 80° reflection accessory. The actual reflection angle was determined to be ≈76.5°. For both measurements, wire grid polarizers (on either ZnSe or BaF_2 substrates) were used to define the polarization. Because the reflection measurement is sensitive to the films on both sides of the wafer, a backside-processing step was used to create uniform organic monolayer-free entrance interfaces. Reflection data were taken both prior to backside processing and after backside processing to ensure the processing conditions did not alter the layers under the metal. The backside-processing step consisted of 5 min UVO, DI rinse, 5 min UVO, DI rinse, 10 s HF dip, DI rinse, and 30 min UVO.

The thickness of the molecular films was determined by spectroscopic ellipsometry (1.2−6.5 eV) at an angle of incidence of 70°. The oxide thickness was determined from freshly UVO cleaned reference films by using a three-phase model (air, SiO_2, Si) and the Si and SiO_2 indices of refraction reported by Herzinger et al. and Brixner, respectively.[24,25] The OTS film thickness was determined from a four-phase model (air, OTS, SiO_2, Si), fixing the oxide thickness at the reference film value and assuming an index of 1.5 for the OTS layer. The thickness for the monolayers directly attached to Si was determined by using an index of refraction of 1.5 and a three-phase model (air, organic, Si). This refractive index value has been used extensively to model the thickness of alkanethiol self-assembled monolayers on gold[26] and silicon[23] and provides a comparison with these well-characterized aliphatic surfaces.

X-ray photoelectron spectra (XPS) were recorded in a commercial ultrahigh vacuum spectrometer (base pressure ≈ 5×10^{-10} Torr, 6.5×10^{-8} Pa) equipped with a monochromatic Al Kα source. Spectra were acquired by using a pass energy of 20 eV yielding an instrumental resolution of 0.3 eV with an internal charge neutralizer operational to minimize surface charging and to ensure observed binding energy shifts were attributable to the changes in local chemical environment. The peaks were fit with a Voigt line shape with a Shirley background correction. It was not necessary to correct the core level binding energies with a rigid shift since the $Au(4f)_{7/2}$ was observed at 84.0 eV and the $Ag(3d)_{5/2}$ was observed at 368.2 eV. Sputtering was performed on a 2 mm by 2 mm area by using an Ar ion source at 2.0 keV with a 50.0 μA extractor current. The pressure during sputtering was ≈5.2×10^{-6} Pa (4×10^{-8} Torr), and spectra were collected at 5 s intervals. The atomic fraction was determined from the integrated peak area and was corrected for the atomic sensitivity factor and electron escape depth.[27]

Atomic force microscope (AFM) images were acquired by using a commercial instrument with a deflection-type scanning head. Contact mode and tapping mode images were acquired in air using Si ultrasharp tips.

To determine how the metal reactivity affects electrical device performance, we have performed current voltage (IV) and capacitance voltage (CV) measurements to characterize vertical diode test structures (see inserts to Figure 14 and Figure 15) fabricated simultaneously with the blank films used for chemical characterization. In contrast to our earlier studies, in which a simple shadow mask-fabricated dot was used to define the device,[21] here a full lithographically defined test structure was employed to enable us to easily vary the device area from (100 μm × 100 μm) to (1 μm × 1 μm) and to avoid possible mechanical damage arising from the probing or packaging of devices over the active region. The area of the molecular junction was defined by etching an opening in a thick (≈160 nm) thermally grown silicon dioxide. The top metal electrode was evaporated through a shadow mask at the same time as the blanket metallization used in the pb-RAIRS measurements. We performed current voltage (IV) and capacitance voltage (CV) measurements on these diode structures with a commercial low-electronic noise probe station.

Results and Discussion

Monolayers under Au. Vibrational spectra prior to and following deposition of 100 nm Au on OTS on oxide and octadecyl monolayers on silicon attached through Si−O−C (aldehyde and alcohol) and Si−C (alkene) covalent linkages are shown in Figure 1. The solid lines of the figure show the p-polarized, Brewster's angle transmission spectra from the double-side-functionalized samples prior to metallization. The dominant features in the C−H stretch region are the methylene symmetric stretch (d+ near 2850 cm^{-1}) and asymmetric stretch (d− near 2920 cm^{-1}). These stretch frequencies can be used to characterize the degree of order of the alkane backbone.[28,29]-Specifically, the d− frequency in highly ordered, all-trans systems is ≈2918 cm^{-1}, while in disordered, liquidlike systems,

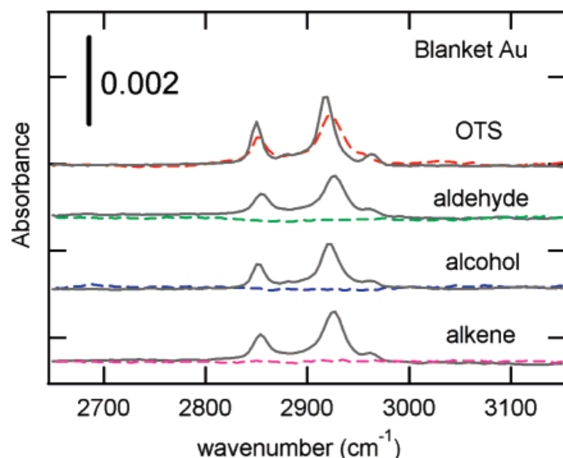

Figure 1. Infrared spectra of organic films under 200 nm of Au. Solid lines are transmission spectra obtained prior to metallization and dashed lines are reflection spectra obtained after treating the backside to ensure that all samples have an identical organic-free entrance face.

it is ≈2928 cm^{-1}. The OTS transmission spectrum exhibits the most intense CH_2 absorption near 2918 cm^{-1} indicating an all-trans extended chain configuration. By comparison, the monolayers directly attached to silicon exhibit a less intense, broader asymmetric CH_2 stretch indicating more conformational defects within the film. The dashed lines in Figure 1 show the spectra obtained from samples after treating the nonmetallized side with UV−ozone and HF to remove any organic layer and to produce a uniform organic-free entrance face for all of the samples. Comparing the spectra acquired after backside processing with the original transmission spectra offers qualitative insights of the structure of the organic monolayer remaining under the deposited Au layer. For the OTS after metallization, the CH_2 asymmetric stretch is shifted to 2923 cm^{-1} and is broader indicating, first, the presence of an organic layer under the Au and, second, that this layer has become more disordered by the Au. For the films directly attached to silicon, there is no evidence of C−H vibrations under the Au metal indicating removal of all of the directly attached organic monolayers, regardless of the attachment chemistry. That is, molecules attached through $(Si)_3Si{-}C$ bonds (alkenes) are equally displaced by the metal when compared with molecules attached through $(Si)_3Si{-}O{-}C$ linkages (aldehyde, alcohol). The OTS is linked to the oxide through a $C{-}Si(OSi)_3$ covalent bond, which should have a similar bond strength to the $C{-}Si(Si)_3$ covalent linkage of the alkene. While the bond strengths of Si−O and Si−C covalent bonds are comparable, previous work has shown the $(Si)_3Si{-}O{-}C$ interface to be more susceptible to oxidation and degradation because of the electron-withdrawing oxygen weakening the Si−Si backbonds.[30,31] The presence of the OTS under the Au and the absence of all of the aliphatic directly attached monolayers indicate that the displacement of the organic monolayers under the Au cannot be attributed solely to differences in chemical linkage. In preliminary studies, the displacement of the C18 from the interface is also observed for $C{-}S{-}Si(Si)_3$ linkages formed from the photoinitiated reaction of 1-octadecanethiol.

Table 1 shows the spectroscopic ellipsometric (SE) thickness, water contact angle (CA), and position and intensity of the CH_2 asymmetric peak in the infrared for the initial films and after metallization. The SE and CA data show that the OTS layer is the thickest and most hydrophobic. The ellipsometric thickness indicates a slightly lower density for the directly attached films, compared to silanization, which has been attributed to packing constraints imposed by the Si lattice.[23] After Au metallization, only OTS monolayers exhibited C−H stretches as seen in Figure 1 and Table 1. To investigate whether the slightly higher molecular density of the OTS relative to the directly attached films (as judged by the greater ellipsometric thickness) is responsible for its reduced reactivity with evaporated Au, less dense OTS films were made which had SE, CA, and IR data comparable to that of the directly attached monolayers and Au was deposited on them. The pb-RAIRS spectra indicated that the OTS monolayer was not displaced despite the lower molecular density. Thus, the apparent displacement of aliphatic chains directly attached to silicon cannot be attributed solely to molecular density.

Figure 2 shows AFM topographical images of approximately 5 nm of Au deposited on H−Si(111), SiO_2, alcohol−Si(111), and OTS−SiO_2. The topography of 5 nm of Au on SiH (Figure 2a) is featureless with a root-mean-square (rms) roughness of 0.4 nm. In contrast, the AFM image of 5 nm of Au on native oxide (Figure 2b) shows large areas partially covered by the Au with individual grains visible on these terraces indicating that gold poorly wets the oxide surface. The step height of the terraces ranges from 15 to 25 nm while the height of the individual grains is on the order of 3 nm with an overall rms roughness of 17−18 nm. The topology of the gold on OTS (Figure 2d) consists of larger grains (≈6−7 nm) in terraces with nearly equivalent step heights (8−11 nm) consistent with a surface that the metal poorly wets. In comparison, the AFM topology of 5 nm of Au on directly attached monolayers (Figure 2c) is largely featureless with an rms roughness of 0.8 nm. The Si-organic monolayers show a gold wetting very different from the OTS-terminated samples and largely similar to the wetting of the H-terminated Si. The actual morphology of the metal layer depends on the physics of deposition conditions such as temperature, rate, and metal thickness; however, the metal was deposited simultaneously for these samples indicating that changes in the morphology can be attributed not to the deposition physics but rather to the properties of the samples. Contrasting the AFM images of the two types of aliphatic surfaces, monolayers on Si−H and SiO_2, illustrates that the Au film morphology is not determined by the outer organic layer.

Shown in Figure 3 are the ellipsometric parameters Ψ and Δ measured for the 5 nm Au films characterized by AFM in Figure 2. Comparing first the native oxide (1.6 nm) and H−Si substrates shows that the overall structure in the visible region (>2 eV) is similar for the two substrates with an offset in Δ because of the presence of the oxide. The d-band edge of the

TABLE 1: Chemical Properties of Organic Monolayers under Au and Ag

	SE[a]	CA[b]	IR-trans[c]		pB-RAIRS Au[c]		pB-RAIRS Ag[c]	
	(nm)	(°)	(cm^{-1})	abs	(cm^{-1})	abs	(cm^{-1})	abs
OTS	2.3	108	2919.9	1.6×10^{-3}	2923.3	1.2×10^{-3}	2923.7	1.5×10^{-3}
aldehyde	1.9	94	2926.8	0.9×10^{-3}			2924.1	0.9×10^{-3}
alkene	2.0	98	2926.1	1.0×10^{-3}			2926.1	1.0×10^{-3}
alcohol	2.0	102	2923.2	1.1×10^{-3}			2924.9	1.2×10^{-3}

[a] $n = 1.50$, ±0.1 nm. [b] ±2°. [c] ±0.2 cm^{-1}, $\pm 5 \times 10^{-5}$.

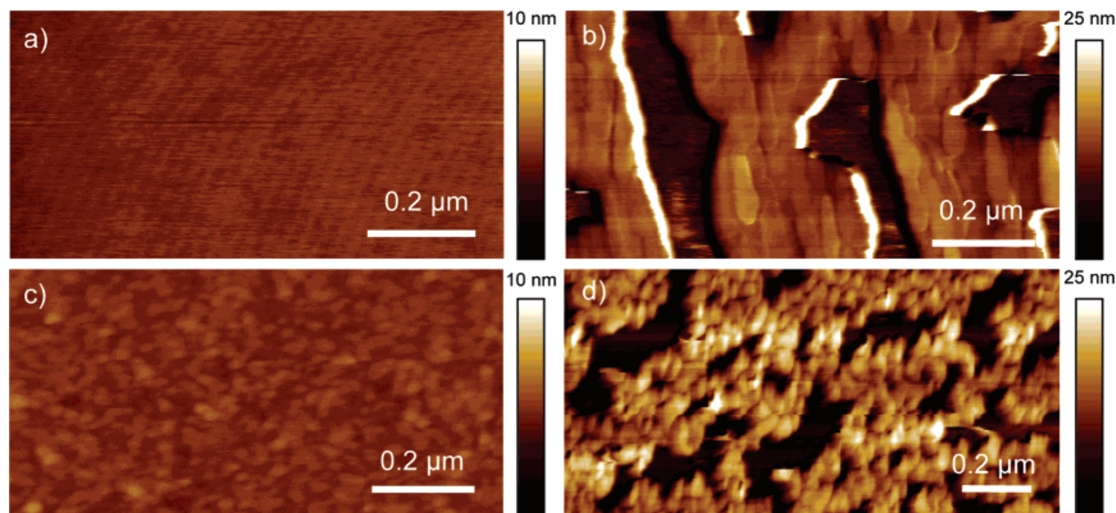

Figure 2. Contact mode AFM of 5 nm of Au on (a) SiH *z*-scale = 10 nm, (b) SiO_2 *z*-scale = 25 nm, (c) alcohol *z*-scale = 10 nm, and (d) OTS *z*-scale = 25 nm.

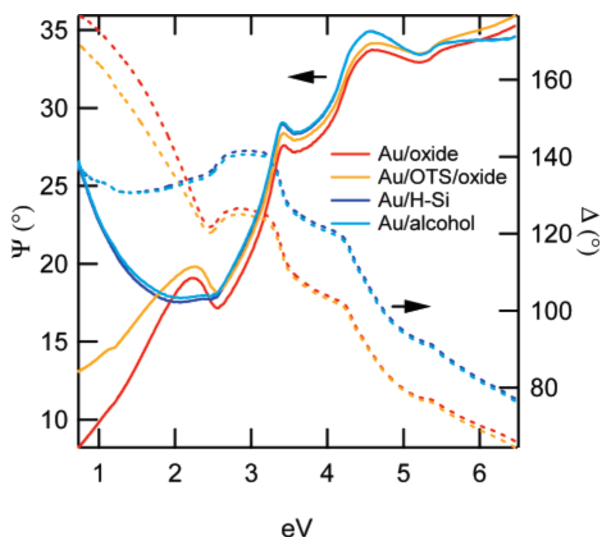

Figure 3. Ellipsometric parameters, Ψ and Δ, obtained from 5 nm of Au on native oxide, OTS−oxide, H−Si(111), and alcohol-terminated Si(111).

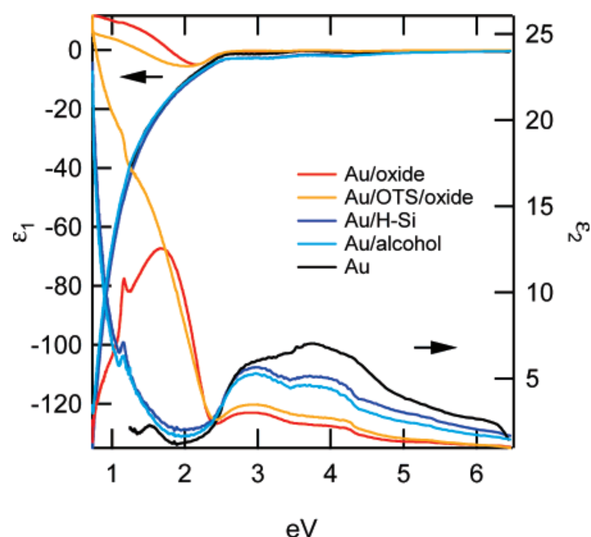

Figure 4. Dielectric constants, ϵ_1 and ϵ_2, obtained from 5 nm of Au on native oxide, OTS−oxide, H−Si(111), and alcohol-terminated Si(111) and dielectric constants from bulk Au.

Au is evident near 2.5 eV and the Si bulk E_1 and E_2 transitions are observed at 3.4 and 4.5 eV. Shown in Figure 4 are the real and imaginary parts of the dielectric function ϵ of the Au film, determined by an Arwin and Aspnes (A&A) analysis of the data.[32] Modeling the Au film thicknesses to minimize the Si substrate features resulted in an 8 nm Au layer on the oxide substrate and a 6 nm Au layer on the H−Si surface. Also shown in Figure 4 is ϵ for a thick (200 nm) vapor-deposited Au film. The ϵ determined for the Au/H−Si is very similar to that of bulk Au, implying uniform wetting of the surface. However, the ϵ for the 5 nm Au film on oxide has a significant plasmon resonance at 1.7 eV, characteristic of Au nanoparticles, indicating incomplete metal wetting of the oxide, consistent with the AFM data shown in Figure 2.

Also shown in Figure 3 are the ellipsometric parameters Ψ and Δ measured for ≈5 nm of Au deposited on the OTS film (2.3 nm) assembled on the native oxide and directly attached alcohol film (1.9 nm) measured in Figure 2. The Ψ and Δ of Au on both the OTS monolayer and oxide surfaces contain a low-energy plasmon response consistent with the nonwetting behavior of Au observed in the AFM images of Figure 2. The Au on alcohol film strongly resembles that of Au on H−Si, suggesting a continuous Au film. This is supported by the ϵ extracted from the A&A analysis, shown in Figure 4.

X-ray photoelectron spectra were obtained as a function of depth following the deposition of 20 nm of Au on SiH, SiO_2, OTS, and directly attached monolayer samples. The Au 4f core binding energy spectra are shown in Figure 5 as a function of sputtering time for Au on alcohol−Si and Au on OTS−oxide. Each spectrum represents approximately 5 s of sputtering with Ar^+ ions. Si first appears in the spectra at ≈55 s (vide infra) implying a Au sputtering rate of ≈0.5 nm/spectrum. The Au 4f peak for both surfaces originally appears at 84.0 eV consistent with bulk gold. After moderate sputtering, a new Au 4f feature appears for the Au−alcohol−Si surface (Au2 in Figure 7a) at 84.8 eV consistent with a reacted Au−Si interfacial region.[33,34] This additional oxidation state is also seen in the depth profile of Au on H-terminated Si. The spectra obtained from the OTS surface shows little evidence of this additional 84.8 eV oxidation state until a significant amount of the bulk Au has been removed. The appearance of a small amount of reacted Au−Si on the OTS sample likely arises from sputtering induced mixing.[27] The C 1s core level spectra for the two molecular surfaces are shown in Figure 6. The C 1s spectra at sputtering time $t = 0$ s are not shown because these spectra are dominated by adventitious

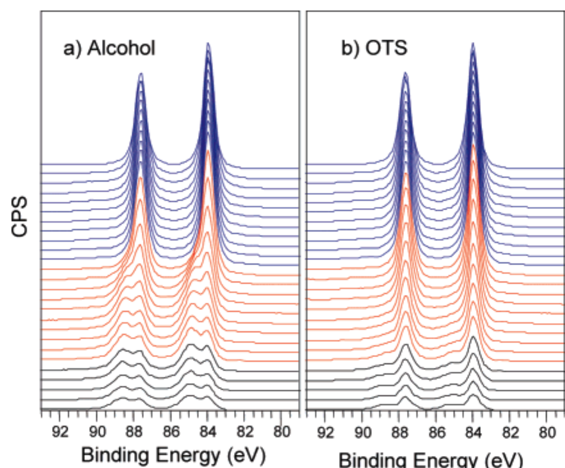

Figure 5. Au 4f core level spectra from ≈20 nm of Au (a) alcohol-terminated Si(111) and (b) OTS terminated native oxide surfaces as a function of sputtering time. Each spectrum was collected after 5 s Ar ion sputtering. Sputtering time from 0 to 50 s shown in blue, from 55 to 100 s in red, and from 110 to 150 s in black.

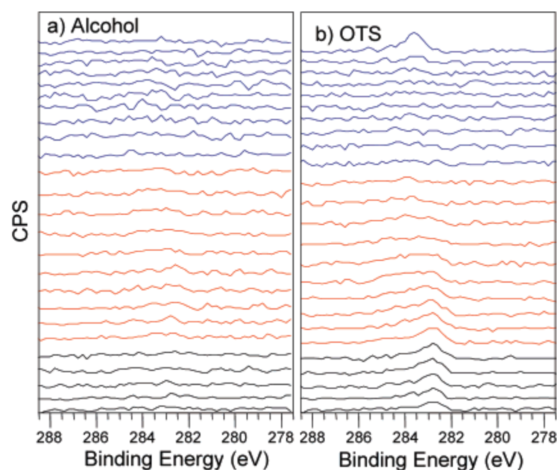

Figure 6. C 1s core-level spectra from ≈20 nm of Au on (a) alcohol-terminated Si(111) and (b) OTS terminated native oxide surfaces as a function of sputtering time. Each spectrum was collected after 5 s Ar ion sputtering. Sputtering time from 5 to 50 s shown in blue, from 55 to 100 s in red, and from 110 to 150 s in black.

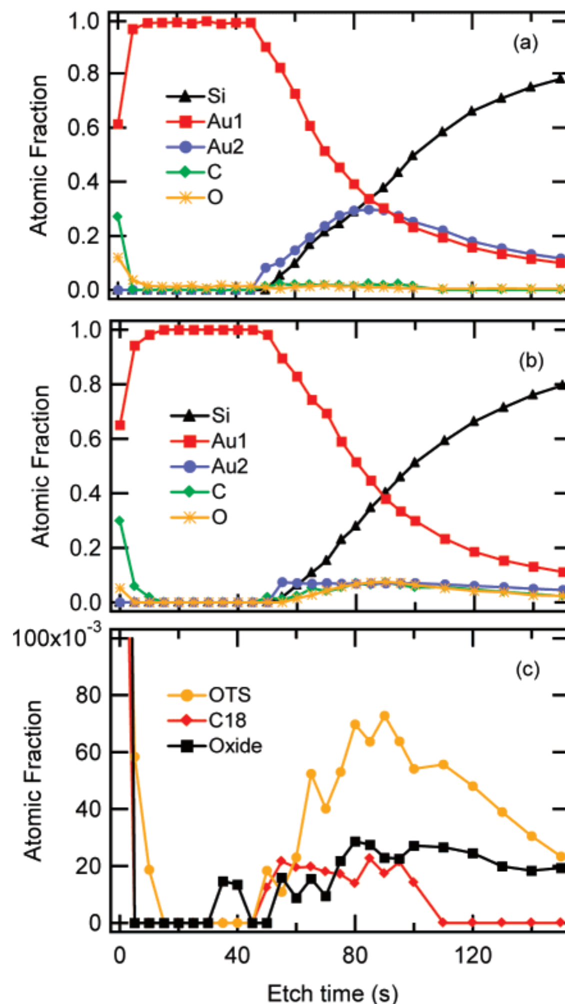

Figure 7. Atomic fraction as a function of sputtering time for (a) Au on alcohol and (b) Au on OTS determined from area fits for each core level spectra and corrected for relative sensitivity. (c) C 1s atomic concentration as a function of sputtering time for OTS, Au on alcohol (C18), and oxide.

carbon. The C 1s intensity increases for the OTS layer at moderate sputtering times and decreases after the interfacial region (see also Figure 7c). Figure 7 shows the atomic fractions as a function of Ar^+ ion sputtering time. For the alcohol monolayer, there is little evidence for carbon at the interface in either Figure 6a or Figure 7c in agreement with the pb-RAIRS data indicating displacement of the monolayer with Au. In fact, the integrated amount of carbon at the alcohol interface is approximately 3 times smaller than the C 1s area seen for the OTS sample and on the order of the C1s signal seen for the native oxide surface (see Figure 7c).

To summarize, the reactivity of aliphatic monolayers with evaporated Au differs significantly for monolayers attached to oxide compared to those directly attached to Si. The infrared (IR) and XPS data indicate that there is no evidence for the directly attached films under the Au in contrast to the OTS films present on oxide. SE and AFM data indicate that Au directly wets attached films and Si−H while it tends to segregate on OTS and oxide monolayers. This indicates that the metal reaction is not determined solely by the molecular layer, but the substrate (i.e., oxide vs Si) is also involved. The displacement of the alkene monolayers, in addition to the alcohol and aldehyde monolayers, under the Au suggests that attachment chemistry differences are not responsible for the displacement of the directly attached monolayers. As seen previously for metal deposited on self-assembled monolayers (SAMs) assembled on Au substrates, the metal often penetrates through the organic monolayer.[1,5,35] In the case of Au, XPS, AFM, and IR, results indicate that OTS monolayers are similar to oxide surfaces while directly attached monolayers are similar to H-terminated silicon surfaces highlighting the importance of the substrate in the reactivity under the metal. Previous work has shown that Au reacts with silicon to form a Au_3Si silicide,[33,34] and the XPS Au core level results are consistent with gold silicide formation. This likely alters the surface chemistry enough to displace the monolayers. It is not clear during which stage this displacement occurs. To test the importance of the metal−Si chemistry, we examined the OTS and directly attached monolayers under evaporated silver, a metal that previously has been shown to not react with silicon[34,36] and can be used as a diffusion barrier for Cu electrical interconnects.[36]

Monolayers under Ag. Figure 8 presents the IR data for OTS, aldehyde, alcohol, and alkene functionalized surfaces with 20 nm of Ag (followed by a 100 nm Au cap). The initial films had similar characteristics to those shown in Figure 1 as shown in Table 1. The pb-RAIRS spectra (dashed lines) indicate dramatic differences in the behavior of Ag with respect to Au

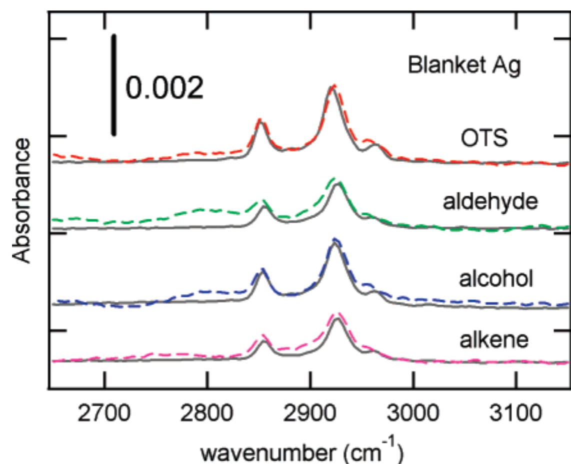

Figure 8. Infrared spectra obtained from organic films under 200 nm of Ag. Solid lines are transmission spectra taken on unmetallized samples, and dashed lines are reflection spectra acquired after backside processing to ensure all samples have an identical organic-free entrance face.

for the directly attached films but similar behavior for the OTS films. For the OTS, there is a slight shift in CH_2 asymmetric stretch to 2923 cm^{-1} (Table 1) indicating that the OTS layer has become slightly disordered by the Ag. The films directly attached to silicon show evidence for organic monolayers under the Ag metal (see also Table 1), for all of the attachment chemistries, in stark contrast to the Au case seen in Figure 1. Additionally, nearly all of the spectra exhibit a tail near 2825 cm^{-1} indicative of a "soft" methylene mode[37] because of the interaction of metal with a CH_2 group suggesting some penetration of the Ag within the organic monolayers.

Figure 9 shows AFM topographical images of 5 nm of Ag deposited on H−Si(111), SiO_2, alcohol-terminated Si(111), and OTS-terminated SiO_2. The topography of 5 nm of Ag on SiH (Figure 9a) contains large smooth terraces with an rms roughness of 2.8 nm. The topology of Ag on an alcohol film (Figure 9c) indicates smaller grains with an image rms roughness about 1.7 nm. The morphology of Ag on oxide and OTS (Figure 9b and 9d) looks very similar to the morphology of Ag on alcohol but with a slightly larger rms roughness, 7.6 and 6.5 nm, respectively, because of a slightly thicker Ag film attributed to the evaporator geometry. In the case of Ag, the metal morphology

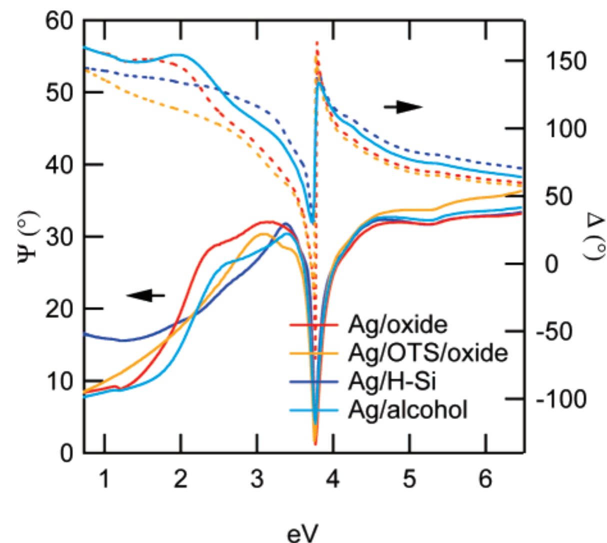

Figure 10. Ellipsometric parameters, Ψ and Δ, obtained from 5 nm of Ag on native oxide, OTS−oxide, H−Si(111), and alcohol-terminated Si(111).

on the directly attached monolayers more closely matches the Ag morphology on the OTS and oxide surfaces, indicating a similar metal wetting for these surfaces, as expected for a metal that does not react with silicon. This does not exclude the possibility of the Ag penetrating the organic monolayer. The subtle topology differences for the two aliphatic surfaces may be due to differences in metal penetration. The fact that the metal layer looks similar on both aliphatic surfaces indicates that Ag, unlike Au, does not have a morphology that is determined by interaction with the substrate. Silver may penetrate the directly attached monolayer, as indicated by the soft mode observed in the IR data of Figure 8, but does not displace the monolayer since it does not react with the substrate. The similar Ag morphology on the two organic monolayers is consistent with the observation of molecular films under the metal and suggests that the Ag wetting behavior, unlike Au, is dominated by interaction with the molecular film and not with the substrate.

Shown in Figure 10 are the ellipsometric parameters Ψ and Δ measured for the ≈5 nm Ag films investigated by AFM in Figure 9. The Ψ and Δ appear qualitatively similar for all of the films, unlike the Au films, and are dominated by the 2D

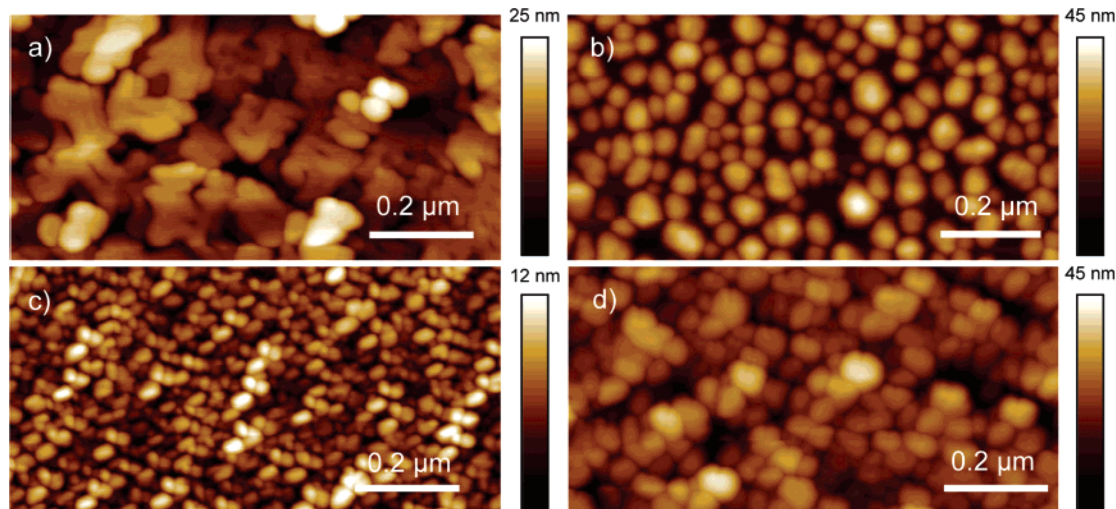

Figure 9. Noncontact mode AFM of 5 nm of Ag on (a) SiH *z*-scale = 25 nm, (b) SiO_2 *z*-scale = 45 nm, (c) alcohol *z*-scale = 12 nm, and (d) OTS *z*-scale = 48 nm.

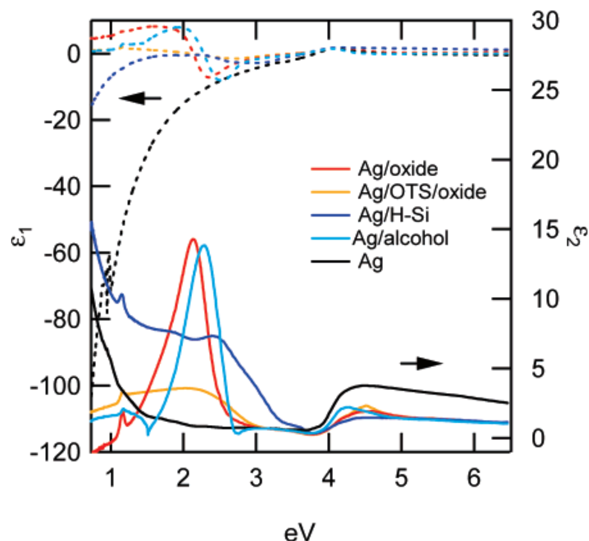

Figure 11. Dielectric constants, ϵ_1 and ϵ_2, obtained from 5 nm of Ag on native oxide, OTS−oxide, H−Si(111), and alcohol-terminated Si-(111) and dielectric constants from bulk Ag.

plasmon near the Ag d-band transition at 3.8 eV. Shown in Figure 11 are the real and imaginary parts of the dielectric function ϵ of the Ag film, determined by an A&A analysis of the data. Modeling the Ag film thickness to minimize substrate features resulted in a Ag thickness of 15 nm on oxide and 12 nm on H−Si. Also shown in Figure 11 is ϵ for a bulk Ag film.[38] The dielectric constants obtained from the Ag films do not resemble the Ag bulk ϵ for either the oxide or the H−Si surfaces. The dielectric constant of the metal film on the oxide has a clear, narrow plasmon resonance at 2.1 eV, indicating a nanostructured film. The dielectric constant of the Ag film on H−Si has a much broader and indistinct feature in the plasmon region, suggesting a partially continuous film as seen in the AFM results of Figure 9. It is clear that the Ag on alcohol film strongly resembles that of Ag on oxide, implying a similar (but smaller) cluster size distribution, while the Ag on OTS film has a weaker, broader plasmon, implying a larger cluster size (with respect to the oxide) and suggesting a more continuous Ag film.

The AFM morphology of Ag (Figure 9) is consistent with the surface plasmon data obtained by using the SE (Figure 11). The Ag grain size was smallest on the alcohol-terminated surface with the corresponding plasmon at the highest energy. On oxide, the Ag clusters were larger and the plasmon frequency was shifted to lower energy. The ϵ of Ag on OTS consists of a broad, indistinct plasmon consistent with the less homogeneous, larger grains observed by AFM. The Ag on H−Si was a partially continuous film with a very broad ϵ. Unlike the case for Au, where the wetting behavior was linked to the underlying substrate, the Ag wetting for both organic films instead seems more closely related to the behavior on the oxide which indicates that the wetting of Ag is independent of substrate interaction, (i.e., silicon vs silicon oxide).

The XPS Ag 3d core level spectra are shown in Figure 12 for 20 nm of Ag on alcohol and OTS as a function of sputtering time. In both cases, the Ag 3d peak occurs at 368.2 eV for all sputtering times, consistent with a metallic Ag binding energy. The observation of only one Ag oxidation state indicates that Ag does not react with the underlying silicon substrate as expected from previous results showing that silicon and silver do not form a silicide.[34,36] Figure 13 shows the atomic fractions for Ag, Si, C, and O as a function of sputtering time for the alcohol and OTS surfaces. The area of the C 1s peak for the

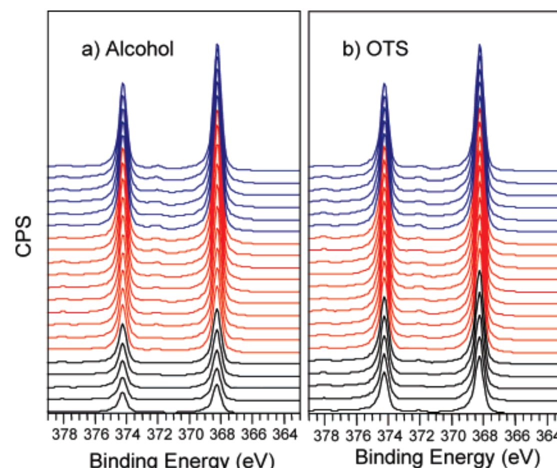

Figure 12. Ag 3d core level spectra from ≈20 nm of Ag on (a) alcohol-terminated Si(111) and (b) OTS terminated native oxide surfaces as a function of sputtering time. Each spectrum was collected after 5 s Ar ion sputtering. Sputtering times of 0−25 s are shown in blue, 30−75 s are shown in red, and 85−125 s are shown in black.

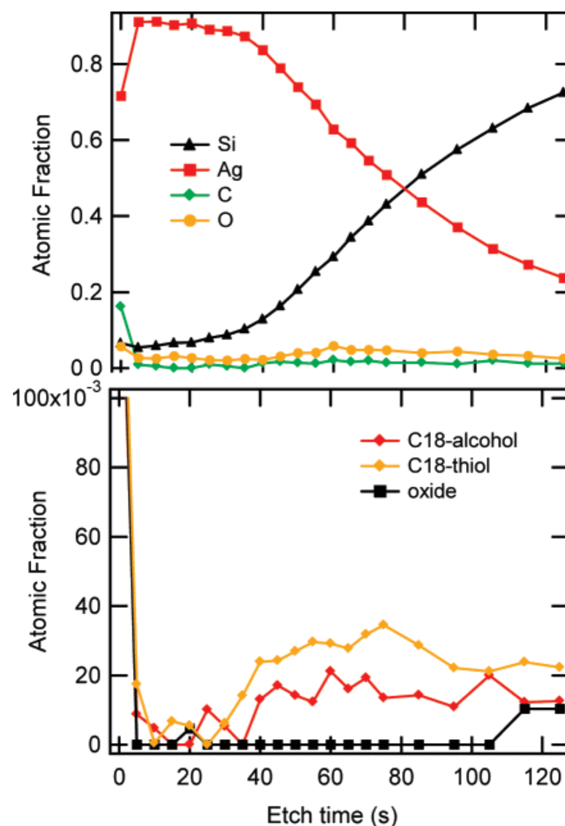

Figure 13. Atomic fraction as a function of sputtering time for (top) Ag on alcohol and (bottom) C 1s atomic concentration as a function of sputtering time for Ag on alcohol (C18) and oxide.

interfacial region (30−75 s) is nearly equivalent for both the alcohol and the OTS in agreement with the observation of organic monolayers under Ag in the IR (Figure 8). From the pb-RAIRS, SE, AFM, and XPS data, Ag appears to react similarly on both aliphatic alcohol and OTS monolayers, unlike Au.

Electrical Device Performance. Shown in Figure 14 are the CV results for Au and Ag deposited on a freshly cleaned thermal oxide of nominally 3.5 nm thickness and on OTS assembled on the identical oxide. CV data was obtained for a series of devices of different areas, and a linear regression of this data with respect to area was performed to extract the capacitance

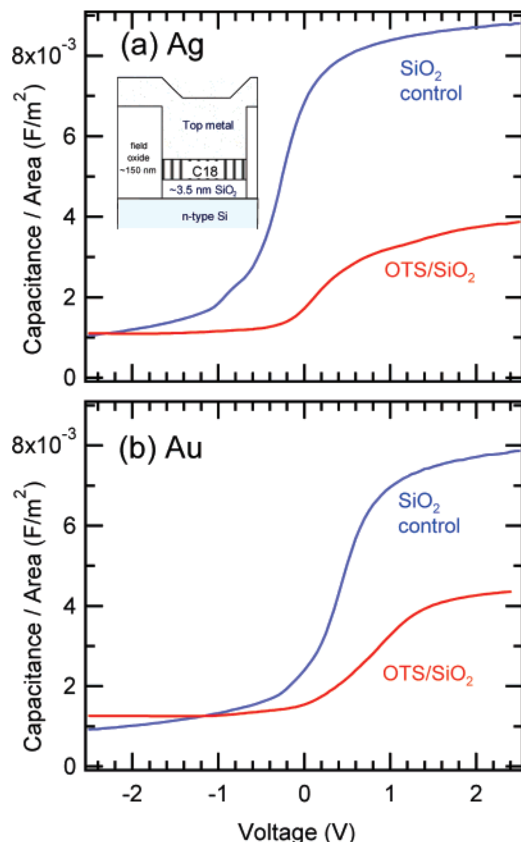

Figure 14. Capacitance per unit area vs voltage measurements (10 kHz) for devices consisting of (a) Ag or (b) Au on a dielectric stack of OTS monolayers on nominally 3.5 nm of SiO_2 on n-type Si (red curves) or control samples of the nominally 3.5 nm of SiO_2 on n-type Si (blue curves). The insert schematically shows the device cross section.

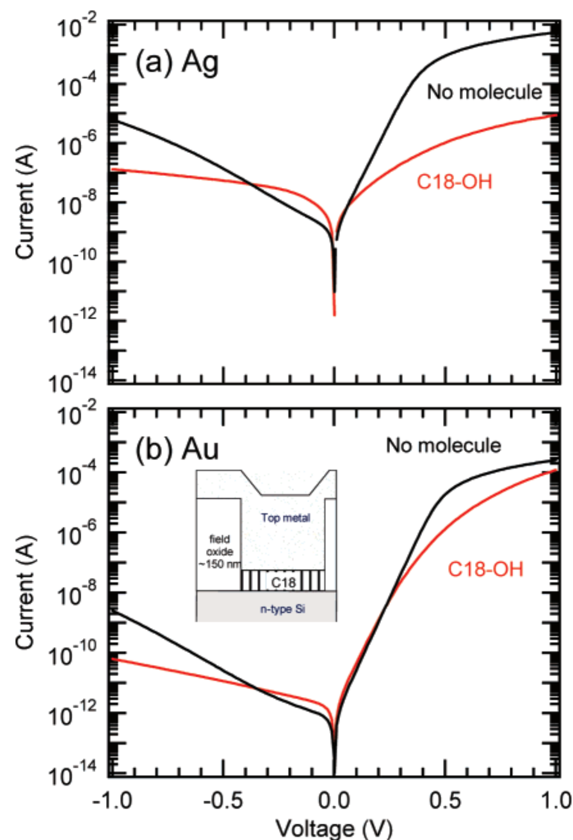

Figure 15. Current vs voltage measurements for devices consisting of (a) Ag or (b) Au on directly attached C18−OH monolayers on n-type Si (red curves) or on H-terminated n-type silicon (black curves). The insert schematically shows the device cross section.

per unit area at each bias voltage and to remove the excess capacitance due to the area of the top electrode that overlaps the thick "field oxide." The two metals behave similarly on OTS, in agreement with the preceding chemical characterization. By using a simple series capacitance model,[39] the dielectric thickness of the OTS film can be extracted for each metal and is found to be ≈2.0 nm under Au and ≈2.7 nm under Ag, in reasonable agreement with the initial film thickness measured by SE shown in Table 1.

The IV results for Au and Ag deposited on the directly attached films and a H-terminated reference are shown in Figure 15. For the Au films, the strong asymmetry in the IV curves is a result of the Schottky barrier arising from the large Fermi level mismatch between Au (5.1 eV) and n-type Si (4.05 eV). The similarity of the IV curves for Au on H-terminated silicon and monolayers directly attached to silicon indicates that the molecular films are not present at the interface in these devices, consistent with the chemical characterization. For the Ag films, the molecular films clearly modify the behavior of the diodes, consistent with the retention of the molecules at the interface. The devices containing molecular monolayers show IV curves that are less rectifying, suggesting a lowering of the Schottky barrier induced by the alkoxy monolayer surface dipole. A quantitative analysis of the IV curves in Figure 15 was not performed because the potential profile is modulated by charge transfer associated with the attachment chemistry and dielectric screening of the films[40] making a simple tunnel barrier model invalid. CV characterization of the directly attached molecules is experimentally hindered by the large dc current in these samples and is dominated by the depletion capacitance of the Si substrate. The results of the electrical measurements indicate that the directly attached monolayers are displaced under Au and are still present under Ag in agreement with the physical and chemical results of the organic monolayers under metal.

Conclusion

When considering the vapor deposition of metals, even nominally inert species such as the noble metals, it is essential to consider the reactivity of the entire system consisting of the substrate, organic monolayer, and top metal. For the case of Au, the reaction of the deposited metal with the Si substrate is responsible for the displacement of the monolayers directly attached to silicon. Ag, a metal that does not react with Si, still preserves the organic monolayers as seen in the XPS, pb-RAIRS, and IV electrical results. The differing reactivity of the organic monolayers with evaporated metal reinforces the need to fully characterize the chemical structure of molecular electronic devices to gain a complete understanding of the electrical response.

Acknowledgment. We wish to thank S. Szeih for assistance in preparation of the OTS films, the NIST Center for Nanoscale Science and Technology Nanofabrication Facility and S. Hsu for use of their respective clean room facilities, and Oleg Kirillov and Monica Edelstein for help with sample preparation.

References and Notes

(1) Walker, A. V.; Tighe, T. B.; Cabarcos, O. M.; Reinard, M. D.; Haynie, B. C.; Uppili, S.; Winograd, N.; Allara, D. L. *J. Am. Chem. Soc.* **2004**, *126* (12), 3954−3963.

(2) Richter, C. A.; Hacker, C. A.; Richter, L. J.; Kirillov, O. A.; Suehle, J. S.; Vogel, E. M. *Solid-State Electron.* **2006**, *50* (6), 1088−1096.

(3) Tai, Y.; Shaporenko, A.; Eck, W.; Grunze, M.; Zharnikov, M. *Appl. Phys. Lett.* **2004**, *85* (25), 6257−6259.

(4) Stewart, D. R.; Ohlberg, D. A. A.; Beck, P. A.; Chen, Y.; Williams, R. S.; Jeppesen, J. O.; Nielsen, K. A.; Stoddart, J. F. *Nano Lett.* **2004**, *4* (1), 133−136.

(5) Jung, D. R.; Czanderna, A. W. *Crit. Rev. Solid State Mater. Sci.* **1994**, *19* (1), 1−54.

(6) DeIonno, E.; Tseng, H. R.; Harvey, D. D.; Stoddart, J. F.; Heath, J. R. *J. Phys. Chem. B* **2006**, *110* (15), 7609−7612.

(7) Chang, S. C.; Li, Z. Y.; Lau, C. N.; Larade, B.; Williams, R. S. *Appl. Phys. Lett.* **2003**, *83* (15), 3198−3200.

(8) Tighe, T. B.; Daniel, T. A.; Zhu, Z. H.; Uppili, S.; Winograd, N.; Allara, D. L. *J. Phys. Chem. B* **2005**, *109* (44), 21006−21014.

(9) Herdt, G. C.; Czanderna, A. W. *J. Vac. Sci. Technol., A* **1999**, *17* (6), 3415−3418.

(10) Jung, D. R.; Czanderna, A. W. *Appl. Surf. Sci.* **1996**, *99* (2), 161−168.

(11) Cai, L. T.; Skulason, H.; Kushmerick, J. G.; Pollack, S. K.; Naciri, J.; Shashidhar, R.; Allara, D. L.; Mallouk, T. E.; Mayer, T. S. *J. Phys. Chem. B* **2004**, *108* (9), 2827−2832.

(12) Lodha, S.; Janes, D. B. *J. Appl. Phys.* **2006**, 100 (2), 024503-1−024503-8.

(13) Metzger, R. M.; Xu, T.; Peterson, I. R. *J. Phys. Chem. B* **2001**, *105* (30), 7280−7290.

(14) Haick, H.; Ambrico, M.; Ligonzo, T.; Tung, R. T.; Cahen, D. *J. Am. Chem. Soc.* **2006**, *128* (21), 6854−6869.

(15) Hooper, A.; Fisher, G. L.; Konstadinidis, K.; Jung, D.; Nguyen, H.; Opila, R.; Collins, R. W.; Winograd, N.; Allara, D. L. *J. Am. Chem. Soc.* **1999**, *121* (35), 8052−8064.

(16) Tai, Y.; Shaporenko, A.; Noda, H.; Grunze, M.; Zharnikov, M. *Adv. Mater.* **2005**, *17* (14), 1745−1749.

(17) de Boer, B.; Frank, M. M.; Chabal, Y. J.; Jiang, W. R.; Garfunkel, E.; Bao, Z. *Langmuir* **2004**, *20* (5), 1539−1542.

(18) Jung, D. R.; Czanderna, A. W.; Herdt, G. C. *J. Vac. Sci. Technol., A* **1996**, *14* (3), 1779−1787.

(19) Konstadinidis, K.; Zhang, P.; Opila, R. L.; Allara, D. L. *Surf. Sci.* **1995**, *338* (1−3), 300−312.

(20) Walker, A. V.; Tighe, T. B.; Haynie, B. C.; Uppili, S.; Winograd, N.; Allara, D. L. *J. Phys. Chem. B* **2005**, *109* (22), 11263−11272.

(21) Richter, C. A.; Hacker, C. A.; Richter, L. J. *J. Phys. Chem. B* **2005**, *109* (46), 21836−21841.

(22) Richter, C. A.; Hacker, C. A.; Richter, L. J.; Vogel, E. M. *Solid-State Electron.* **2004**, *48* (10−11), 1747−1752.

(23) Hacker, C. A.; Anderson, K. A.; Richter, L. J.; Richter, C. A. *Langmuir* **2005**, *21* (3), 882−889.

(24) Herzinger, C. M.; Johs, B.; McGahan, W. A.; Woollam, J. A.; Paulson, W. *J. Appl. Phys.* **1998**, *83* (6), 3323−3336.

(25) Brixner, B. *J. Opt. Soc. Am.* **1965**, *55*, 1205.

(26) Shi, J.; Hong, B.; Parikh, A. N.; Collins, R. W.; Allara, D. L. *Chem. Phys. Lett.* **1995**, *246* (1−2), 90−94.

(27) Hofman, S. *Rep. Prog. Phys.* **1998**, *61*, 827−888.

(28) Macphail, R. A.; Strauss, H. L.; Snyder, R. G.; Elliger, C. A. *J. Phys. Chem.* **1984**, *88* (3), 334−341.

(29) Snyder, R. G.; Strauss, H. L.; Elliger, C. A. *J. Phys. Chem.* **1982**, *86* (26), 5145−5150.

(30) Haber, J. A.; Lewis, N. S. *J. Phys. Chem. B* **2002**, *106* (14), 3639−3656.

(31) Bazant, V.; Chvalovsky, V.; Rathousky, J. *Organosilicon Sompounds*; Academic Press: New York, 1965.

(32) Arwin, H.; Aspnes, D. E. *Thin Solid Films* **1984**, *113*, 101−113.

(33) Yeh, J. J.; Hwang, J.; Bertness, K.; Friedman, D. J.; Cao, R.; Lindau, I. *Phys. Rev. Lett.* **1993**, *70* (24), 3768−3771.

(34) O'Shea, J. N.; Phillips, M. A.; Taylor, M. D. R.; Beton, P. H.; Moriarty, P.; Kanai, M.; Dennis, T. J. S.; Dhanak, V. R.; Patel, S.; Poolton, N. *J. Chem. Phys.* **2003**, *119* (24), 13046−13052.

(35) Walker, A. V.; Tighe, T. B.; Stapleton, J.; Haynie, B. C.; Upilli, S.; Allara, D. L.; Winograd, N. *Appl. Phys. Lett.* **2004**, *84* (20), 4008−4010.

(36) Yukawa, M.; Kitagawa, H.; Iida, S. *Appl. Surf. Sci.* **2004**, *237* (1−4), 156−160.

(37) Yamamoto, M.; Sakurai, Y.; Hosoi, Y.; Ishii, H.; Ito, E.; Kajikawa, K.; Ouchi, Y.; Seki, K. *Surf. Sci.* **1999**, *428*, 388−392.

(38) Palik, E. D. *Handbook of Optical Constants of Solids II*; Academic Press: New York, 1991.

(39) Richter, C. A.; Stewart, D. R.; Ohlberg, D. A. A.; Williams, R. S. *Appl. Phys. A: Mater. Sci. Process.* **2005**, *80* (6), 1355−1362.

(40) Lodha, S.; Carpenter, P.; Janes, D. B. *J. Appl. Phys.* **2006**, *99* (2), 024510.